*Work supported in part by the National Science Foundation under Grant. No. 545-782-46.

[1]M. Fixman, J. Chem. Phys. 36, 310 (1962).
[2]K. Kawasaki, Phys. Rev. 150, 291 (1966).
[3]L. P. Kadanoff and J. Swift, Phys. Rev. 166, 89 (1968); J. Swift, *ibid.* 173, 257 (1968).
[4]K. Kawasaki, Ann. Phys. (N.Y.) 61, 1 (1970); in *Proceedings of the International Summer School of Physics "Enrico Fermi," Varenna, Italy*, 1970 (Academic, New York to be published).
[5]H. Mori, Progr. Theoret. Phys. (Kyoto) 33, 423 (1965).
[6]P. Berge *et al.*, Phys. Rev. Letters 23, 693 (1969); 24, 1223 (1970); D. L. Henry *et al.*, *ibid.* 25, 1170 (1970).
[7]For more general discussion of the gross variables, see M. S. Green, J. Chem. Phys. 20, 1281; (1952) 22, 398 (1954), as well as Ref. 4.
[8]J. V. Sengers, in *Proceedings of the Critical Phenomena Conference, Washington, D.C.*, 1965, edited by M. S. Green and J. V. Sengers, Natl. Bur. Std. (U.S.) Misc. Pub. No. 273 (U. S. GPO, Washington, D. C., 1966); in *Proceedings of the International Summer School of Physics "Enrico Fermi," Varenna, Italy*, 1970 (Academic, New York, to be published).
[9]The same result was also obtained recently by Ferrell using the fluctuation-dissipation theorem. See R. A. Farrell, Phys. Rev. Letters 24, 1169 (1970).
[10]P. Résibois (private communication).
[11]H. L. Swinney (private communication).

PHYSICAL REVIEW A VOLUME 5, NUMBER 1 JANUARY 1972

Persistent-Current Measurements of the Superfluid Density and Critical Velocity*†

James R. Clow‡ and John D. Reppy§
Department of Physics, Yale University, New Haven, Connecticut 26528
(Received 12 March 1971)

Gyroscopic measurements of superfluid persistent currents in liquid helium below and near the λ transition are presented here. Measurements were conducted in a variety of sizes of porous material from 0.05- to 150-μ average size. Near the λ transition, both the superfluid density ρ_s/ρ and the critical velocity ω_c exhibit a $\frac{2}{3}$-power dependence on the temperature difference from the transition. A depression of the λ transition is observed for both ρ_s/ρ and ω_c in the smallest pores. Data for ρ_s/ρ and ω_c away from the transition and down to about 1.25 °K are given and are in agreement with measurements made by other methods.

I. INTRODUCTION

Persistent currents in superfluid helium have been examined extensively since their prediction and discovery.[1-4] This paper will discuss the superfluid critical velocity ω_c and the superfluid density ρ_s/ρ in the region of the superfluid–normal-fluid phase transition.[5,6] Near the λ point both of these quantities exhibit a simple-power-law behavior.

There is a wide class of second-order transitions exhibiting a λ specific-heat anomaly at a critical temperature T_c. One can discuss their thermodynamic functions in terms of an order parameter η that vanishes at T_c.[7] The scaling-law approach[8,9] postulates that $\eta = \eta_0(T - T_c)^{\xi}$ near T_c. Although the details of the singularity are not known, it is still possible to determine various relations between their critical exponents. Consider the λ point in liquid helium. Measurements of the specific heat[10] show a logarithmic dependence on the temperature difference from the λ point. The scaling-law approach leads to a connection between the temperature dependence of the specific heat and the superfluid density with a critical exponent of $\frac{2}{3}$ for the superfluid density.[11]

Persistent-current critical velocities discussed in this paper have the same general properties as those obtained by pressure-vs–flow-rate studies.[12] That is, they are temperature independent away from the λ point, and they increase inversely with channel size. Near the λ point the situation is quite different. The critical velocity is independent of channel size and is proportional to $(T_\lambda - T)^{2/3}$. Langer and Fisher[13] have arrived at a critical velocity exponent of $\frac{2}{3}$. They consider the flowing superfluid to be a metastable state which, because of critical fluctuations, breaks up into vortex rings. Their argument leads to a critical velocity proportional to ρ_s/ρ and hence a $\frac{2}{3}$-power-law behavior.

II. EXPERIMENTAL METHOD

One of the most intriguing things about superfluid helium is its similarity to a superconductor. A given ring of superconductor will trap a magnetic field because of a persistent circulation of current in the superconductor. It remains essentially as long as the ring is superconducting and the critical field is not exceeded. Onnes first detected such persistent currents by placing the ring in an external magnetic field and observing the torque produced. The mechanical analog for a superfluid persistent current is shown schematically in Fig. 1. An externally applied rotation of velocity $\vec{\omega}$ is applied to the vector angular momentum $\vec{L}_p$ of the

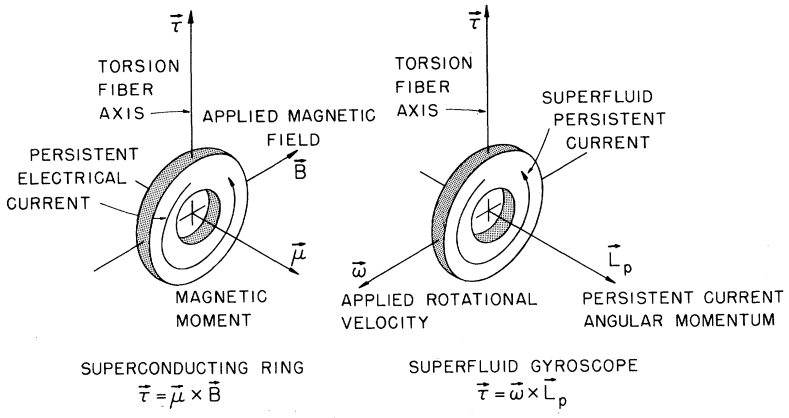

FIG. 1. Nondestructive detection of persistent currents.

fluid current. This results in a torque $\vec{\tau} = \vec{\omega} \times \vec{L}_p$ which is readily measured by an angular deflection of the torsion fiber. The method is nondestructive to the superfluid persistent current (so long as ω is not excessive) and is referred to as a superfluid gyroscope.[14]

The fact that superfluid persistent currents can and do exist in superfluid helium makes the actual construction of such a gyroscope feasible.[15] In the case of the superconducting ring, there is a maximum field for a given temperature and material for which the ring remains in the superconducting state. This is in a sense a phase boundary. For the superfluid persistent current there is also a critical velocity of rotation ω_c (which depends on channel size and temperature near the λ transition) which can also be thought of as a phase boundary. ω_c separates the ω, T half-plane into two regions, one which is nondissipative (allowing persistent currents of a characteristic angular velocity ω_s which are "frozen in" and are relatively stable), and a dissipative region where there is either only normal fluid (i.e., $T > T_\lambda$) or at least strong coupling between the normal and superfluid components allowing dissipation. The latter is the region ($T < T_\lambda$ and $\omega > \omega_c$) in Fig. 2. There appear to be just two ways to obtain the isorotational state characterized by ω_s: (a) Applying, starting from $\omega = 0$ and $T < T_\lambda$, a rotational velocity $\omega > \omega_c$ to the container. As long as $\omega > \omega_c$ the superfluid will come into equilibrium with the rotating container. As the applied rotation ω is reduced to zero, the superfluid of velocity ω_s just less than ω_c will remain. (b) Starting with the temperature above the λ temperature at an applied velocity ω and cooling leaves the superfluid state in rotation with a velocity $\omega_s = \omega$ if $\omega < \omega_c$. In both cases the superfluid is left with the velocity it had when the critical velocity curve was crossed. Hence, the formation of the superfluid state with $\omega_s \neq 0$ is intimately related to what happens on the critical velocity curve. One cannot permanently change the velocity of the superfluid without crossing ω_c.[16] In case (a), if the final applied velocity ω was less than ω_c, then the superfluid would end up with a value of $\omega_s = 0$ after ω was reduced to zero.

Measurements of the torque yield several kinds of useful information about superfluid helium. Consider Fig. 3(a). A current of velocity ω_s is created by rotation about the cylinder axis while cooling to some value of temperature well below the λ point. Then, a measurement of torque is made by applying a rotation $\vec{\omega}$ perpendicular to the fiber axis and the angular momentum vector $\vec{L}_p$. Therefore, $\tau = k\theta = \omega L_p$. The effective torsion constant is k. θ is the angular deflection, and ω is the rotational velocity applied to produce the torque τ. L_p is proportional to the product $\rho_s \omega_s$ with a constant of proportionality C involving the effective moment of inertia of the fluid. Thus we have

$$\theta = (C\,\omega\omega_s/k)\rho_s\,,$$

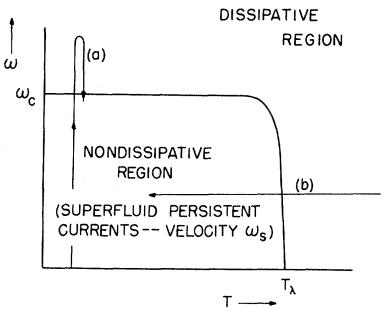

FIG. 2. Shows how the ω, T half-plane can be considered to be divided into two regions by the critical velocity curve. One region ($\omega < \omega_c$; $T < T_\lambda$) is nondissipative to stable persistent currents, and the other ($\omega > \omega_c$ or $T > T_\lambda$) is where dissipation can occur. (a) Shows how a persistent current can be created by exceeding ω_c at a constant temperature away from T_λ. (b) Shows how a persistent current characterized by a velocity $\omega_s < \omega_c$ can be created by cooling while steadily rotating at a velocity $\omega = \omega_s$.

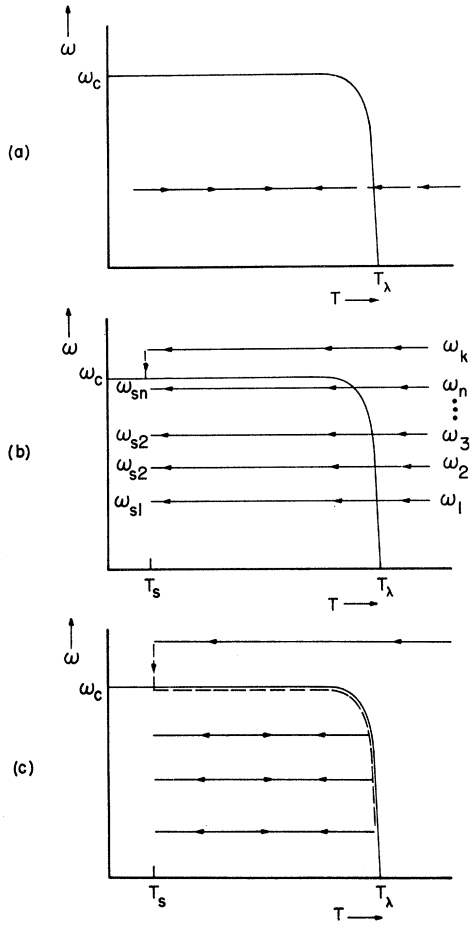

FIG. 3. Principal methods of measurement of ρ_s and ω_c. (a) A persistent current of velocity $\omega_s < \omega_c$ is "frozen-in" by rotating while cooling through the λ point. The superfluid velocity ω_s remains constant for all temperatures below T_λ. Only ρ_s varies with temperature, so we can measure $\rho_s(T)$ for any value of ω_s below the critical curve. (b) A sequence of velocities ω_{sn} are obtained corresponding to different currents, and L_p proportional to ω_s for the n different currents are measured at a fixed temperature $T_s \ll T_\lambda$. When the value of ω_c is exceeded, excess current is dissipated leaving the same velocity $\omega_s = \omega_c$ for all applied rotational speeds ω greater than ω_c. This is method I, and gives ω_c for the temperature T_s. (c) A single current with velocity $\omega_s = \omega_c$ is created and measured at T_s. Continuous measurements are then made of critical angular momentum L_{pc} as T approaches T_λ. Since $\rho_s(T)$ is known and is found to be independent of velocity to first order, the torque measured gives the critical angular momentum L_{pc} which is proportional to the product $\rho_s(T_n)\omega_c(T)$. Simple division by $\rho_s(T)$ therefore gives the temperature dependence of $\omega_c(T)$. This is method II, and is used where ω_c is flat and where ω_c is steep but still large. Method III is used where it is steep and small (very close to T_λ). It is described as follows. Cooling from various temperatures T_n near T_λ to T_s, where ρ_s is large, enables us to measure the current where it is proportional to the product $\rho_s(T_s)\omega_c(T_n)$ instead of the product $\rho_s(T_n)\omega_c(T_n)$ where it is too small to be measured. Necessary to this method is the fact that ω_s does not change with temperature below the critical curve.

where the quantity in parens contains only constants that are temperature independent. Hence we have a direct measure of ρ_s temperature dependence for any velocity ω_s, and as long as the critical curve is not crossed we can even approach the λ temperature T_λ. Figure 3(b) shows another use for torque measurements. A sequence of currents is created as described above by rotating and cooling to a fixed temperature T_s well below T_λ and then are measured there. Here ρ_s is constant for each current so we have persistent-current angular momenta L_p proportional to ω_s and the value of ω applied to create the current. So we get essentially $L_p = I\omega$ or "solid body" type of rotation as is observed above T_λ or in any ordinary fluid in rotation. If $\omega > \omega_c$, then $L_p = I\omega_c$ for all such ω. So the critical velocity is readily identified as the value of ω for which saturation of L_p occurs.[17] This could in principle be done at each temperature less than the λ temperature, and would enable us to map out the temperature dependence of the critical velocity $\omega_c(T)$. Figure 3(c), however, gives an alternative method for obtaining $\omega_c(T)$. First, ω_c is identified for some standard value of temperature T_s as just described. A current of velocity $\omega_c(T_s)$ is created by cooling while rotating at a velocity $\omega > \omega_c(T_s)$. Then the temperature is allowed slowly to approach T_λ where ω_c is monotonically decreasing with temperature. Continuous measurements of θ now give the temperature dependence of the product of ρ_s and ω_s. But $\rho_s(T)$ is known, so division by it gives $\omega_c(T) = \omega_s(T)$. Cooling from a sequence of temperatures $T_1, T_2, \cdots, T_n$, all near T_λ to a standard temperature T_s and making measurements there, has the added advantage of increasing ρ_s to $\rho_s(T_s)$ which is large. This increases the deflection angle θ corresponding to $\omega_s = \omega_c$ for the temperatures $T_1, T_2, \cdots, T_n$. We thus make measurements of θ where it is large. Then making use of the fact that ω_s remains constant in the nondissipative region below the ω_c curve, we obtain the value of ω_c where ρ_s is very small. A sequence of values of ω_c obtained in this way is independent of the measurement of $\rho_s(T)$ since it is always measured at the same value of temperature T_s.

III. EXPERIMENTAL APPARATUS

The gyroscope (Fig. 4) consists of a torus-shaped thin-walled magnesium bucket container A with rectangular cross section. It is filled with a spongelike filler B such as Scott Foam or Metricel filter material, with accurately known pore sizes.[18] It is centered by a dozen small brass screws D on a light magnesium support ring G which has a diameter about $\frac{1}{16}$ in. less than the innermost dimension of the bucket container. Through two 0.020-in. holes on opposite sides of the support ring, a horizontal torsion fiber C made of 0.0015-

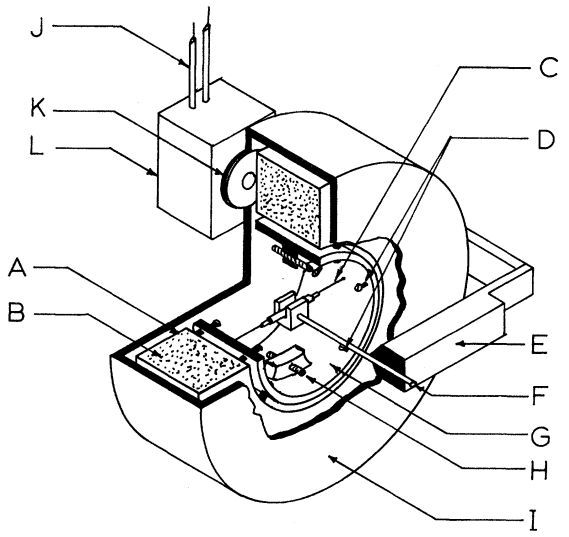

FIG. 4. Gyroscope. Parts shown are A, the bucket; B, the spongelike filler; C, the fiber; D, the ring centering screws; E, the yoke; F, the fiber support rod; G, the support ring; H, horizontal balance adjustment; I, the hydrodynamic shield; J, the transducer leads; K, the detector coil; L, the nonmetallic block to support the coil and determine a 90° turn of the bucket from horizontal to vertical.

in. tungsten wire has been stretched and held in place against slippage by two countersunk set screws (not shown). The fiber rests in the fiber support rod F which is mounted in a yoke E that can in turn be used to rotate the bucket container from the position shown to one with the cylindrical axis vertical. In the latter position, rotation about the vertical while cooling produces a persistent current. A plastic shell I shields the torus from the gross effects of stirring of the helium, but allows several degrees of free swing inside with about a millimeter clearance at all points. A small nonmetalic block L containing an adjustable coil form K is used to hold a coil and determine mechanically a 90° turn of the shell from the horizontal to the vertical position. The shell rides (because of friction) with the bucket support rod, but once in a vertical or horizontal position, continuation of the motion overrides the friction and allows adjustment of the position of the bucket within the shell. Since the coil was found to be position sensitive to the silverings of the inner Dewar, a brass can (not shown) encloses the entire gyroscope assembly to electrically shield it.

The fiber is centered and glued in a 0.010-in. slot in the fiber support rod only after the bucket and ring assembly has been carefully balanced on the fiber. Such balance, tested by placing the fiber across a pair of tweezers used as a fulcrum, is accomplished by centering of the ring on the 00-90 screws, placing of small pieces of tape on the ring between it and the bucket, and by adjusting the horizontal balance screws. The period of the bucket can easily be made greater than 10 sec, and 12–14 sec is quite satisfactory. This leaves the center of gravity of the assembly about 0.0015 cm from the fiber axis, and gives a gravity contribution of about 15% to the effective torsion constant. The computed value of k without this gravity effect is 98.5 dyn cm for a fiber of 0.49 in. length.

A modified Colpitts oscillator is used as a position detector in measuring an angle change of the bucket about the fiber axis. As the metal of the bucket approaches the sensing coil (K of Fig. 4) consisting of 13 turns of No. 31 copper wire, the frequency changes. This change is calibrated over a uniform 90° rotation of the bucket to give a plot of frequency versus angle. The frequency during normal operation is about 7.15 MHz, but during the calibration changes from 6.90 to 7.50 MHz, depending on the position of the bucket. The sensitivity $s = d\theta/df$ is also frequency dependent and is used to convert to angle changes from frequency changes. It is known less accurately because it is obtained graphically by differentiation of the θ-vs-f curve. Several of the capacitors of the Colpitts oscillator circuit that determine the frequency and isolate the transistor from the frequency determining part of the circuit are placed in the helium for stability. The transistor and associated resistors, however, are in the vacuum can (Fig. 5) and no means is provided to keep their tempera-

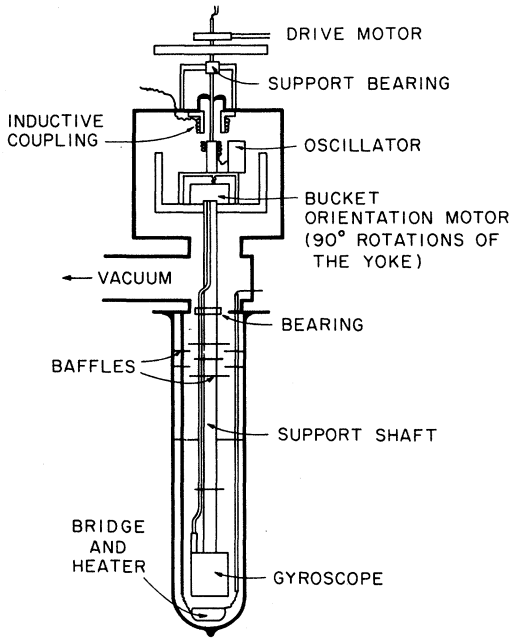

FIG. 5. Schematic of the apparatus showing the cryostat and major features of the rotating system.

ture constant. The typical drift is about 10–15 cycles in a 10-min period when running with helium in the Dewar. The oscillator drifts much more at nitrogen temperatures where there is no superfluid to keep the frequency determining components constant. Drift of 10–15 cycles in a 10-min period is unimportant as long as it is constant and can be effectively subtracted out. The frequency is picked up inductively (Fig. 5) from the rotating system, amplified, and counted by a Hewlett-Packard 524b frequency counter. The frequency counts were displayed as a function of time on a Brown strip-chart recorder. By selecting a short gate time one can observe the noise, check the damping, or examine the extent of balance on the fiber. If one selects longer periods of counting, periodic variations tend to average out. Most data points were obtained by counting for 10-sec intervals, and these were averaged over many counts to prevent any one count from weighing heavily. An average value of f or Δf was accepted only if it remained constant over many repeated countings.

Other main features of the rotating system and cryostat are shown schematically in Fig. 5. The system is suspended from the top by a $\frac{1}{4}$-in.-diam shaft containing leads to the 90° rotation motor. Alignment is obtained about midway with a $1\frac{1}{2}$-in. roller bearing at the lowest room-temperature point. From here down the shaft is unrestrained and can propagate vibrations. Fortunately the fiber itself is highly selective as to what frequencies it will propagate to the bucket, but the relative placement of these bearings has significance in obtaining the lowest mechanical noise level. Further, the runs that give the least noise (as low as 30 cps) seem to be connected with those times when extreme care was taken to obtain good balance on the fiber. Different buckets each having the same physical dimensions, but having different weights and moments of inertia, seem to have different minimum vibrational noise characteristics. The motors used to drive the system were two in number. A 1-rpm Borg synchronous motor was used with an electric clutch to obtain reproducible measurement speeds. A Bodine variable speed dc motor was used with a series of different timing belts and pulleys to provide speeds up to 200 rpm for creating persistent currents. Two large flywheels (Fig. 5) were used to insure that the rotations were as uniform as possible.

IV. GYROSCOPE MECHANICS

So far, our discussion has been confined to measurements of temperature dependences of ρ_s and ω_c without regard for their absolute values. Absolute values can be estimated and used to compare data of different fibers, data runs, and pore sizes. In measuring the output frequency difference between clockwise and counterclockwise rotations Δf, we see that

$$\Delta f = (2\omega/ks)L_p = (2\omega/ks)I\omega_s ,$$

where ω is 1 rpm. s we know certainly to 5%. I, the effective moment of inertia of the superfluid-bucket system, we do not know because of possible contributions from backflow around the fibers of the filler material, and due to a lack of precise knowledge about the geometry of the currents. But we can make some guesses. The spring constant can be estimated also to probably 10–20%. We do this based on the following considerations. The effective center of gravity of the bucket is not quite coincident with the axis of the fiber, so it acts as a physical pendulum of length l, and an effective mass m (reduced by the buoyant force of the helium). Estimates of the length l can be made from the period measurements of the bucket on the fiber in both the horizontal and vertical position of the fiber. For the fiber in the vertical position there is no physical pendulum, just a torsional one. From the formula for the period of a torsional pendulum $T = 2\pi(I/k)^{1/2}$, we obtain the following expression for the length:

$$l = (k/mg)[(T_v/T_h)^2 - 1] ,$$

where k is the torsion constant of the fiber material, m is the real mass of the bucket plus ring, and T_v and T_h are the vertical and horizontal fiber periods in seconds. The results for the various buckets are given in Table I.

Alignment of the center of suspension of the gyroscope with the rotation axis is never perfect either so we must allow the possibility that there is a distance a between them. This leads to a general solution (allowing for fluid damping of the container) consisting of three terms:

$$\theta = \theta_T + \theta_c + \theta_p .$$

θ_T is a damped sinusoidal term or transient that goes to zero as the time gets large. θ_c is the centrifugal force term

$$\theta_c = \frac{a\omega^2}{g - \omega^2 l + k/ml} ,$$

and θ_p is the deflection due to a persistent current

$$\theta_p = \omega L_p/[(k + mgl) - ml^2\omega^2] .$$

TABLE I. Bucket suspension data.

Bucket (μ)	Mass (g)	T_v (sec)	T_h (sec)	l (cm)
10.00	8.52	2.41	2.25	0.001 18
0.20	12.96	2.97	2.71	0.001 49
1.20	11.20	2.80	2.37	0.003 61

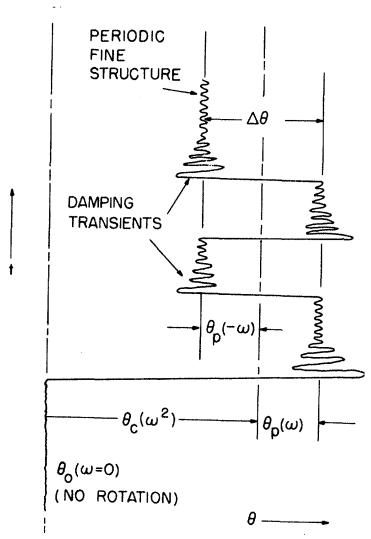

FIG. 6. Time sequence of angular deflections of the bucket with indicated contributions due to the centrifugal force θ_c, the persistent currents $\theta_p(\pm\omega)$, transients, and the periodic fine structure due to imperfect alignment with the vertical.

All of these contributions to the motion are seen during a typical measurement, and are shown schematically in Fig. 6. We first rotate in a positive direction $(+\omega)$, wait until damping stops the container, then rotate in a negative direction $(-\omega)$, wait, and repeat. Since the centrifugal term depends on ω^2, it is independent of whether ω is positive or negative. We thus measure $\Delta\theta = 2|\theta_p|$ which gives us L_p if we know the quantity $(k+mgl - m\omega^2 l^2)$, the effective torsion constant. The value of m is about 10 g; the value of ω is about 0.1 rad/sec, and l is about 0.001 cm. Therefore we have $m\omega^2 l^2 \ll k+mgl$ and it can be neglected with respect to it. Table II gives the effective torsion constant $(k+mgl)$ and other pertinent data for comparison of currents created at 10 rpm and measured at

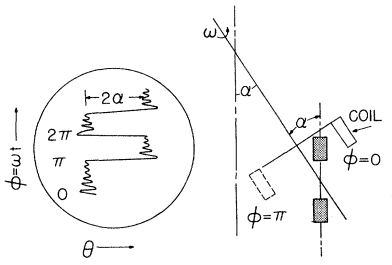

FIG. 7. Origin of the periodic fine structure due to nonperfect alignment of the rotational axis with the vertical. During each complete turn the bucket flips from one side to the other and back as it tries to remain vertical. It is constrained by the fiber to swing only in a back and forth direction relative to the coil detector.

TABLE II. Absolute magnitude estimates of persistent-current angular momenta L_p with torsion constants and sensitivities used to obtain these estimates.

Bucket (μ)	Δf (10^{-3} mc)	s (rad/mc)	$(k+mgl)$ (g cm^2/sec^2)	L_p (g cm^2/sec)
0.20	4.0	0.520	117.2	1.15
1.20	4.4	0.826	137.5	2.38
10.00	3.1	0.448	118.2	0.78

$\Delta T = (T_\lambda - T) = 100$ m °K. Assuming that L_p can be estimated by the formula $L_p = \frac{1}{2}\pi h(R_2^4 - R_1^4)\rho_s \times$(percent open volume), then we obtain a classical solid-body estimate for L_p of 1.80 g cm^2/sec. This value of L_p agrees with the values of L_p determined from actual deflections to an order of magnitude. The latter are given in Table II.

Although our measurements do not contain the parameter a explicitly, its presence is a possible source of error. Vibrations can cause small perturbations in a and, hence, the centrifugal term may not be strictly constant. It is made worse by faster measurement rates because of the ω^2 dependence, but better by a smaller value of l. Hence, again we see that the balance of the gyroscope on the fiber is important.

There is at least one effect that keeps the transient term for dying out completely (aside from the vibrational noise) and is present at all times. That is the inability to align the axis of rotation vertically, as shown schematically in Fig. 7. The bucket is essentially $2b\sin\alpha$ farther away from the coil at its farthest point than at its closest point. The mean radius of the bucket is b; the angle of misalignment is α. Since the bucket is constrained by the horizontal fiber to move back and forth only, relative to the coil, it will flop back and forth once each rotational period. Unless the rotational rate is very slow, there is insufficient time for the transient term to damp out. We cannot eliminate this effect by even the most careful balancing of the platform so we make it as good as possible, i.e., $2\alpha \cong 10^{-4}$ rad and take as the average value the geometric center or mean of the periodic behavior.

V. THERMOMETRY AND TEMPERATURE CONTROL

The temperature during operation of this experiment was limited to the range between 1.25 °K and $T_\lambda = 2.172$ °K, so no special modification of the usual liquid-helium apparatus was necessary.

Temperature measurement and control was achieved by means of an ac Wheatstone bridge used not only to measure the resistance of a temperature sensor, but also to control a feedback of current to a bath heater and match the heat input to that removed by the vacuum pumping system.

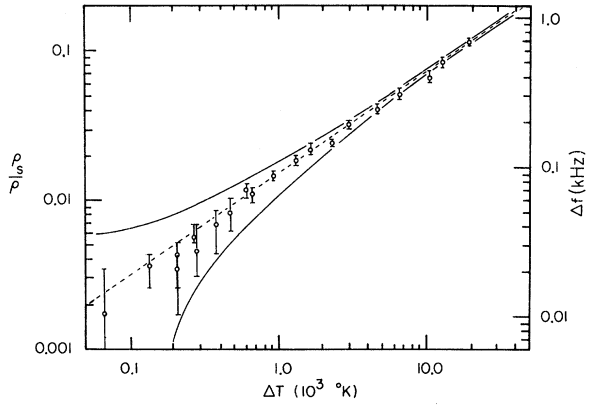

FIG. 8. ρ_s/ρ from run I of Table III—very near T_λ. Open circles shown are data obtained by averaging several values of Δf at a given temperature. Error bars shown are fixed by the extreme values used in the averaging. Dotted line is of slope $\frac{2}{3}$ and passes through the point ($\Delta f = 0.108$ kc, $\Delta T = 1.34 \times 10^{-3}$ °K) which is used to normalize this run. Solid lines show how a 20-cps constant error in measurement of Δf proportional to $(\Delta T)^{2/3}$ would appear on such a plot. Note that the error on the lower side is favored on a log-log plot—and that the data tend to fall somewhat below the dotted line as might be expected.

This keeps the vapor pressure constant, and hence the temperature of the bath. A calibration of the temperature sensor was made with an oil manometer and the 1958 temperature scale (T_{58}), with the assumed absolute temperature resolution of about 1 m °K.[19] Temperature differences from T_λ can be made with considerably higher precision, however, because the measurement of resistance of the sensor R at T_λ undergoes a slope discontinuity and is readily identified to a very small percent of the total resistance $R = R_\lambda$.[20]

The sensor was a doped germanium resistor with a value of $R_\lambda = 1234.17\ \Omega$ at T_λ. Cycling to room temperature has little effect on thermometers of this type. The power input was always less than 28×10^{-9} W. The heater received approximately 2.5×10^{-3} W. The temperature was maintained constant to about 6.7×10^{-6} °K when within a few millidegrees of T_λ and to about 2.0×10^{-4} °K when near $T = 1.40$ °K. Under these conditions we notice about a 4-μW power input fluctuation per microdegree change in bath temperature. The time constant of the servo system was adjusted so as to cause a fluctuation in temperature to damp to half its value in about $\frac{1}{2}$ min. Equilibrium to the constancy quoted above usually attains in less than 10 min from the time a change in temperature is initiated.

Two heaters were used, one near the gyroscope and one near the thermometer. The system behaved identically to within 1 μdeg regardless of which one was used. This is as might be expected because of the large effective thermal conductivity of the superfluid.

The value of R_λ or the resistance at the λ point was found to drift about 20 μdeg in an 8-h interval, so this has been taken as our estimate of the best temperature resolution during a given data run. An additional shift of R_λ that can be corrected for is due to the change of pressure of the liquid helium above the sensor as the liquid evaporates. This corresponds to a temperature shift $\Delta T_\lambda = -1.087 \times 10^{-6}$ °K/cm or about a 20-μdeg shift higher of T_λ in temperature during a 20-h run.

The gyroscope itself, however, may not respond as quickly to temperature changes as the bulk liquid. Although it is submerged, thermal contact is through a superleak, and through the metallic walls of the container. The best measure of this response time is to change the temperature quickly to some

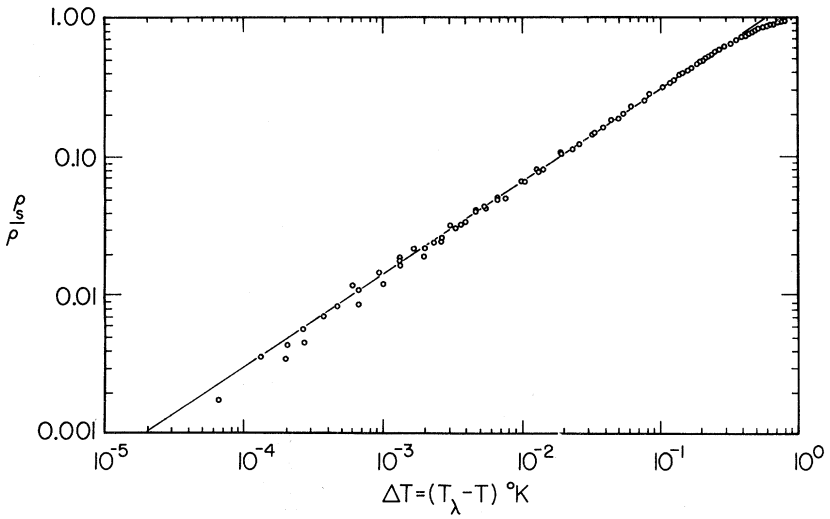

FIG. 9. Values of ρ_s/ρ for the 10.0-μ channel size bucket are plotted as a function of $\Delta T = (T_\lambda - T)$. Slope of the solid line is $\frac{2}{3}$. In the region about 100 mdeg below T_λ, the data are consistent with a power law $\rho_s/\rho = A(T_\lambda - T)^a$, where $A = 1.438$ and $a = 0.67 \pm 0.03$.

TABLE III. ρ_s/ρ is expressed in percent. T is in degrees Kelvin, and ΔT is in m°K. The data all were obtained using the 10.0-μ bucket. The current in each case was created by rotating at 12 rpm and cooling to the lowest temperature obtainable. Data were taken in the order presented, after a closest approach was made to T_λ.

ΔT	T	ρ_s/ρ
	I	
0.6106		1.16
0.2080		0.427
0.2751		0.444
0.3758		0.683
0.4764		0.819
0.6777		1.09
0.9461		1.43
1.684		2.13
3.026		3.18
4.704		4.03
6.717		4.95
13.0		8.19
19.7		10.98
10.065		6.42
1.34		1.84
0.2684		0.563
2.349		2.36
0.2013		0.341
0.1342		0.358
0.0671		0.171
	II	
0.671		0.824
1.342		1.7901
2.013		2.2113
2.684		2.4219
3.691		3.2643
5.368		4.3173
6.710	2.1653	4.7386
10.065	2.1619	6.5287
14.5	2.1575	8.1082
23.8	2.1482	11.3725
32.7	2.1393	14.9528
51.5	2.1205	18.7436
84.8	2.0872	28.1154
143.1	2.0287	38.8561
255.1	1.9169	54.7566
	III	
1.342	2.1707	1.572
2.684	2.1693	2.536
4.697	2.1673	3.956
6.710	2.1653	4.889
13.420	2.1586	7.760
26.5	2.1455	12.274
45.0	2.1270	18.157
62.5	2.1095	23.026
119.0	2.0530	34.792
169.4	2.0026	43.415
214.3	1.9577	50.312
255.3	1.9167	55.993
293.5	1.8785	60.557
328.5	1.8435	63.702

TABLE III. (*Continued*)

ΔT	T	ρ_s/ρ
360.5	1.8115	67.252
390.7	1.7813	70.396
481.8	1.7532	72.425
445.4	1.7266	75.062
470.0	1.7020	77.091
493.0	1.6790	78.613
515.8	1.6562	80.084
536.1	1.6359	81.250
564.1	1.6079	83.279
590.6	1.5814	84.445
639.3	1.5327	87.235
680.7	1.4913	88.959
720.2	1.4518	90.582
752.1	1.4199	91.799
783.2	1.3888	92.814
801.5	1.3705	93.625
825.3	1.3467	94.437
844.5	1.3275	94.842
864.7	1.3073	95.248
864.7	1.3073	95.451
882.4	1.2896	96.263
896.4	1.2756	96.364
	IV	
1.0065	2.17099	1.138
2.0130	2.16999	1.857
3.3617	2.16864	2.995
4.0260	2.16797	3.354
5.7102	2.1663	4.133
10.065	2.1619	6.588
19.7	2.1523	10.062
32.7	2.1393	14.495
39.0	2.1330	16.771
54.0	2.1180	20.245
78.0	2.0940	25.875
105.0	2.0670	32.104
124.8	2.0482	35.458
143.5	2.0285	38.812
156.3	2.0157	41.208
179.9	1.9921	45.401
191.3	1.9807	46.838
205.0	1.9650	48.635
224.4	1.9476	51.510
235.3	1.9367	52.947
245.8	1.9262	54.445
265.5	1.9065	56.781
274.9	1.8971	57.979
283.7	1.8883	58.937
302.1	1.8699	61.333
311.0	1.8610	62.291
319.6	1.8524	63.249
336.4	1.8356	65.286
344.3	1.8277	66.124
352.5	1.8195	67.202
368.5	1.8035	68.041
376.1	1.7959	69.059
383.6	1.7884	69.838
398.1	1.7739	71.215
404.8	1.7672	71.635
411.7	1.7603	72.233
425.0	1.7470	74.030

TABLE III. (*Continued*)

ΔT	T	ρ_s/ρ
431.9	1.7401	74.390
438.0	1.7340	74.510
450.8	1.7212	75.827
457.5	1.7145	75.588
464.1	1.7079	75.827
476.0	1.6960	76.606
481.0	1.6910	77.205
504.3	1.6677	79.301
526.6	1.6454	80.619
546.3	1.6257	81.877
550.1	1.6219	83.015
617.4	1.5546	86.069
701.8	1.4702	90.082
736.7	1.4353	91.340
769.3	1.4027	92.418
789.0	1.3830	93.017
834.7	1.3373	94.515
856.0	1.3160	95.173
870.2	1.3018	95.353
893.3	1.2787	96.551
909.3	1.2627	96.311

new value and see how quickly L_p stops changing. Such tests showed that the same value of L_p was established whether the temperature change was from above or below, and within the time the servo came to equilibrium. We conclude that the temperature measurement is certainly better than 1%, and probably the best known quantity we measure.

VI. MEASUREMENTS OF ρ_s/ρ

The data presented here consist of four runs labeled I, II, III, and IV in Table III. The data was obtained from the 10.00-μ bucket, and for each case from a single persistent current. Data runs II–IV are in the same fiber, and are just a few days apart in measurement. Period measurements indicate that the effective torsion constant for each of these runs remained the same. Each current was created by rotating 12 rpm, and cooling through T_λ. An initial approach to a temperature very near T_λ (and higher in temperature than to be made subsequently) insured that we have left only a current that is stable in the range of lower temperatures to be measured. That is, no further critical velocity attentuation will occur. The order used in the presentation of the data is the order in which the measurements were made. The data has been normalized to the accepted theoretical value of 92.55% at 1.40 °K as obtained by Bendt, Cowan, and Yarnell.[21]

The normalization procedure is explained as follows. Runs II–IV are normalized at 1.40 °K. For these, the data were plotted on an expanded scale to obtain the best value of N from the relation $N\Delta f_{1.40\,^\circ\mathrm{K}} = 92.55$. The values of N for each of these runs are $N_{\mathrm{II}} = 10.1436$, $N_{\mathrm{III}} = 11.9790$, and $N_{\mathrm{IV}} = 10.5301$. Division of the ρ_s/ρ data given in Table III by the values of N gives the frequency difference Δf in kilocycles from which the normalized data were obtained. The data from run I, i.e., the data very near the λ point, were normalized at $\Delta T = (T_\lambda - T) = 1.34$ mdeg, to the comprehensive data from runs II–IV. The normalization constant N_{I} is 1.7065. Because the magnitude of the deflections is small near T_λ, the data of run I given in Table III are averages over several measurements made at each temperature. The error bars shown in Fig. 8 are the most extreme of the values averaged, and is a suitable way of estimating the resolution of Δf in kilocycles, or ρ_s/ρ in percent. Figure 9 demonstrates the $\frac{2}{3}$ power dependence on ΔT of ρ_s/ρ near the λ point. Away from the λ point, the values of ρ_s/ρ have a scatter of about $\frac{1}{2}$% over the whole range measure. If the data are normalized to the data of Dash and Taylor[22] (instead of to Bendt, Cowan, and Yarnell's theoretical value), ours lies on top of theirs and agrees completely. The disagreement between the two curves with different normalization is about 1% at 1.40 °K.

Measurement of ρ_s in very small pores seems to

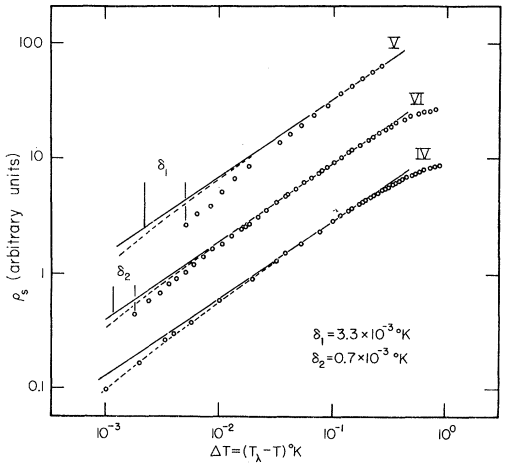

FIG. 10. Unnormalized ρ_s data for three channel sizes are compared in arbitrary units as a function of $\Delta T = (T_\lambda - T)$. The data for curves V and VI corresponding to channel sizes of 0.05 and 0.20μ, respectively, clearly depart from the $\frac{2}{3}$-power behavior as T_λ is approached. Solid lines are of slope $\frac{2}{3}$ and are normalized at ΔT approximately 200 mdeg, where the small depression of T_λ can be considered negligible. Standard error of 30 cps corresponding to the minimum angular resolution is given as the dotted lines. Curve IV is for the 10.0-μ channel size bucket, and agrees with the $\frac{2}{3}$-power behavior to within the acceptable error. A depression of the λ point of 3.3×10^{-3} and 0.7×10^{-3} °K is indicated for curves V and VI, respectively.

TABLE IV. Run V gives ρ_s in 0.05-μ pores and is in arbitrary units (actual recorded values of Δf). Run VI gives ρ_s in 0.20-μ pores and shows the reversibility of ρ_s. The temperature difference $\Delta T = (T_\lambda - T)$ is in mdeg.

ΔT	ρ_s
V	
119.9	11.59
5.386	0.22
6.71	0.28
8.723	0.32
11.41	0.42
14.5	0.56
19.5	0.71
36.0	1.12
45.0	1.35
56.8	1.61
73.8	1.97
96.4	2.32
122.6	3.09
158.4	3.41
191.0	4.03
234.2	4.60
289.1	5.23
112.6	2.73
VI	
417.3	12.05
330.0	10.54
255.0	9.12
167.9	7.05
91.1	4.76
45.0	2.94
19.6	1.60
6.71	0.74
3.355	0.405
2.013	0.27
2.684	0.35
4.026	0.495
4.710	0.55
5.704	0.62
6.71	0.71
8.052	0.85
9.73	0.99
12.07	1.10
14.5	1.31
17.8	1.455
21.0	1.63
21.0	1.61
24.5	1.87
29.6	2.13
36.5	2.50
44.0	2.83
53.4	3.26
62.4	3.69
73.7	4.13
84.8	4.475
101.4	5.04
117.4	5.56
117.4	5.62
135.4	6.09
135.4	6.07
157.7	6.76
198.0	7.70
235.0	8.58
292.1	9.93
292.1	9.89
374.5	11.29
491.3	12.90
552.3	13.70
622.5	14.37
728.8	15.04
809.2	15.52
877.6	15.78
911.2	15.91

depart from the $\frac{2}{3}$ power dependence. Measurements of specific heat in small pores[23] indicate a possible depression of the λ temperature relative to that occurring in the bath, so we suggest this possibility for ρ_s as well as for ω_c the critical velocity. Table IV gives Δf corresponding to ρ_s for two persistent currents in very small pores. The pore sizes are 0.05 and 0.20μ, respectively. Since it is uncertain how to normalize this data we make no attempt. Figure 10 gives a plot of this data together with a single current run IV from the 10.0-μ bucket for comparison. The data of run IV in the 10.0-μ material have some scatter at the smallest values of ΔT but agrees with the $\frac{2}{3}$ power dependence to within the standard 30 cps error bar. The data for the 0.20 and 0.05-μ bucket lie 50 and 150 cycles outside the standard error shown. This corresponds to about a 0.7×10^{-3} and 3.3×10^{-3} °K λ-point depression, respectively. Best values of ΔT_λ the λ-point depression are determined from a plot of $\Delta f^{3/2}$ vs ΔT. The intercept is ΔT_λ. Obtained this way $\Delta T_\lambda = (0.70 \pm 0.2) \times 10^{-3}$ °K and $\Delta T_\lambda = (3.2 \pm 0.2) \times 10^{-3}$ °K for the data of Table IV, labeled runs V and VI, respectively. Note in particular the high degree of reproducibility of run V. The data were taken in the order given in the table, and approximately twelve hours elapsed time. During this time a considerable variation of ΔT and consequent change of ρ_s was executed. These currents were created in like manner to those in the 10.0-μ bucket and consequently should have nearly the same value of angular velocity associated with the superfluid.

VII. MEASUREMENTS OF ω_c

The data presented in this section are obtained by the three methods described earlier and depicted in Fig. 3. Away from T_λ, ω_c is found to be nearly temperature independent, and increases as the dimension of the channel decreases. This

TABLE V. Conversion of critical angular velocities ω_c to linear critical velocities v_c for the buckets with various pore size filler material. $v_c = r\omega_c$ where $r = 2.0$ cm.

Bucket (μ)	ω_c (at $\Delta T = 250$ m °K) (rad/sec)	v_c (cm/sec)	d (after compression) (cm)	$v_c d$ (cm^2/sec)
150	0.48	0.96	150×10^{-4}	1.44×10^{-2}
10	1.05	2.09	7.36×10^{-4}	1.48×10^{-3}
1.20	3.67	7.34	0.83×10^{-4}	6.05×10^{-4}
0.20	>14.3	>28.6	0.14×10^{-4}	$>3.98\times10^{-4}$

agrees with pressure-flow studies for flow through small channels, where v_c, the linear critical velocity is found to obey approximately the relation $v_c d = 10^{-3}$, (cf. Ref. 12). We can in fact make a direct comparison with the information of Table V. Method I was [as described in Fig. 3(a)] used to obtain the data where possible to do so. That is, a sequence of persistent-current angular momenta L_p were determined at a fixed temperature T_s away from T_λ, corresponding to creation velocity ω. ω_c is the value of ω where L_p departs from being proportional to ω and saturates. For this comparison we use our mean bucket radius of 2.0 cm and the relation $v = r\omega$, since L_p is proportional to ω and suggests solid-body rotation. Data included are for the 150-, 10-, and 1.20-μ buckets (Table V). For the 0.20- and 0.05-μ buckets, the saturation velocity ω_c is well above any rotational rate obtainable safely with our present apparatus. L_p for these buckets was demonstrated to be proportional to ω (away from T_λ) for all speeds obtainable. Figure 11 shows data for the 10.0-μ bucket.

The 0.20-μ bucket demonstrates methods II and III clearly [see Figs. 3(b) and 3(c)]. Figure 12 is a plot of $\log(L_p)$ vs $\log\Delta T$, where $\Delta T = (T_\lambda - T)$. It is recalled that L_p is proportional to the product of ρ_s and ω_s. Since both ρ_s and ω_c decrease very rapidly near T_λ, a plot of this type makes the change more gradual. Also, when ω_s is constant and less than ω_c, the ρ_s temperature dependence is apparent as a straight line of slope $\frac{2}{3}$. A nonlinear L_p will mean a changing ω_s or a current attentuation with temperature. Simple division of the critical angular momentum L_{pc} by ρ_s gives the temperature dependence of the critical angular velocity ω_c.

In the region very near T_λ, where the deflection angle is so small as to correspond to less than $\Delta f = 30$ cps, the minimum angular resolution of the transducer detector, we resort to method III

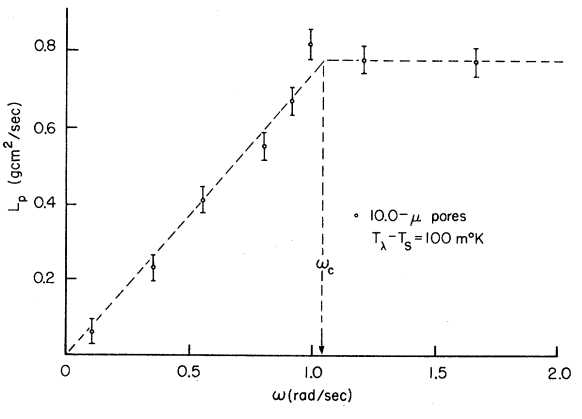

FIG. 11. Angular momentum L_p of persistent currents formed by rotating at an initial velocity ω while cooling through T_λ to a temperature T_s 100 mdeg below T_λ. At T_s the rotation is stopped and L_p measured. ω_c is thus determined by method I described in Fig. 3.

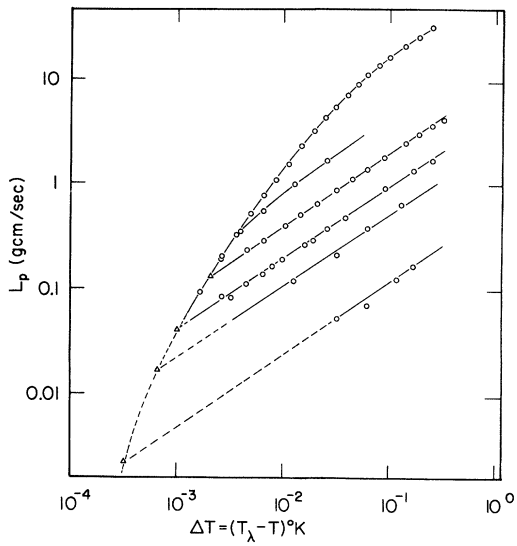

FIG. 12. Values of angular momentum are plotted as a function of $\Delta T = (T_\lambda - T)$ for just two persistent currents. Each of the straight lines of slope $\frac{2}{3}$ are reversible functions of temperature and demonstrate measurement of L_p for different constant velocities ω_s. The critical angular momentum curve can be divided by the temperature-dependent ρ_s/ρ to obtain the temperature dependence of ω_c (method II). Additional points on the critical angular momentum curve corresponding to T_m, temperatures of closest approach, can be fixed by measuring the current where it is large and extrapolating with the known ρ_s/ρ. These points are the open triangles.

TABLE VI. Critical angular-velocity data. Away from T_λ, method I is used to determine the critical velocity. The temperature dependence is then measured by method II where possible. Very near T_λ, where the angular momentum of the current is small, method III is used. Data obtained by method III are denoted by an asterisk (*) in the table. The data for the 0.20-μ bucket are corrected 0.5 mdeg for a depressed λ point. The curvature of the data for which this correction has not been made is evident in Fig. 13.

$(T_\lambda - T)$ (mdeg)	ω_c (rad/sec)
150-μ bucket	
663	0.482
583	0.486
433	0.482
333	0.486
245	0.486
183	0.502
145	0.492
98	0.512
53	0.482
28	0.532
11.2	0.526
6.87	0.516
4.08	0.462
2.85	0.540
1.79	0.540
1.43	0.570
1.39	0.560
6.50	0.470
4.95	0.493
2.35	0.417
1.6	0.47
0.5	0.482
0.075	0.45
0.04	0.503
0.029	0.468
0.02	0.487
0.015	0.45
0.005	0.383
10-μ bucket	
180	1.05
115	0.995
100	1.05
77	0.984
61	0.974
46	0.995
37	0.932
28	0.963
20.5	0.869
14.7	0.817
11.4	0.764
7.3	0.773
4.75	0.712
1.9	0.628
1.0	0.545*
0.94	0.555*
1.0	0.440*
0.64	0.429*
0.36	0.319*
0.405	0.283*
0.26	0.251*
0.19	0.230*
0.145	0.204*
0.068	0.152*
1.20-μ bucket	
715	3.77
680	3.82
620	3.72
515	3.77
480	3.82
420	3.77
380	3.87
345	3.72
285	3.67
240	3.72
208	3.64
168	3.80
138	3.61
118	3.61
88	3.51
68	3.40
50	3.46
38	3.48
29.2	3.04
23.5	2.83
17.5	2.83
13.2	2.72
10.0	2.51
7.3	2.41
5.4	2.30
4.0	2.04
3.0	1.83
2.3	1.83
1.7	1.47
1.2	1.38
0.86	1.15
0.67	1.05
0.47	0.942
0.47	0.859
0.30	0.754*
0.24	0.702*
0.15	0.576*
0.20-μ bucket	
79.5	13.72
64.5	13.51
52.5	12.46
41.5	11.73
32.0	11.0
25.0	9.84
20.0	8.59
16.0	7.44
11.2	6.07
8.5	5.13
6.3	4.40
4.8	3.61

TABLE VI. (*Continued*)

$(T_\lambda - T)$ (mdeg)	ω_c (rad/sec)
3.4	2.83
2.2	2.15*
1.75	1.76*
0.67	0.95*
0.40	0.62*
0.19	0.41*
0.11	0.293*

entirely.[24] Here a sequence of L_p were measured at T_s well away from T_λ (i.e., $T_\lambda - T_s = 250$ mdeg) corresponding to a sequence of values T_m, the temperatures of closest approach. This determines $\omega_c(T_n)$. Knowledge of $\rho_s(T)$ is not necessary since measurements were made only at T_s where $\rho_s(T)$ becomes $\rho_s(T_s)$, a constant. That is L_p is proportional to ω_c only at a constant T_s. We denote all data obtained this way be an asterisk (*) in Table VI.

Figure 13 shows a linear plot of ω_c within a couple of tenths of a degree of T_λ. In all moderately small channels, the critical velocity is flat and independent of temperature away from T_λ. In the smallest channels ω_c seems to sense the approach of the transition at a lower temperature than do the larger ones. Data for the 0.05- and 0.20-μ buckets indicates an intrinsic critical velocity independent of channel size very near the λ point, and is essentially a measure of that temperature dependence. It is found to be proportional to $(T_\lambda - T)^{2/3}$ or pro-

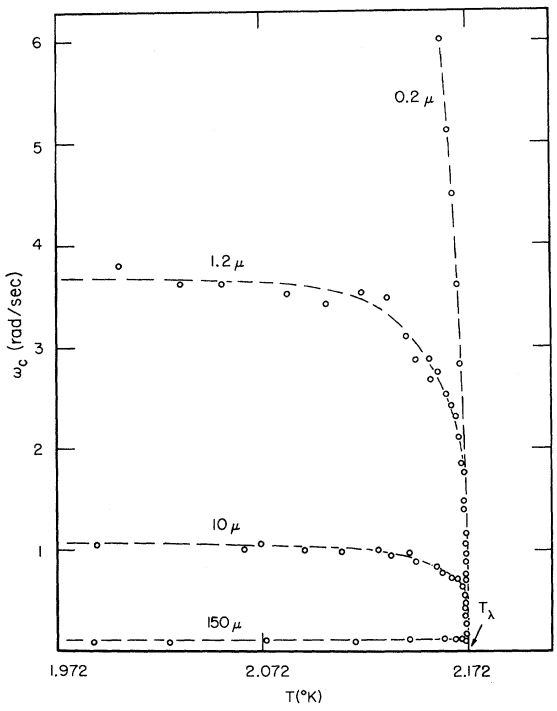

FIG. 13. Critical velocities ω_c for several channel sizes are plotted on a linear scale as a function of absolute temperature a few tenths of a degree below T_λ. Away from T_λ, ω_c is larger in smaller channel sizes. The smaller the channels, the lower the temperature at which ω_c begins to depart from being flat. The 0.20-μ channel data are the steepest shown and is a measure of the size-independent critical velocity curve that the other data approach and appear to join near T_λ.

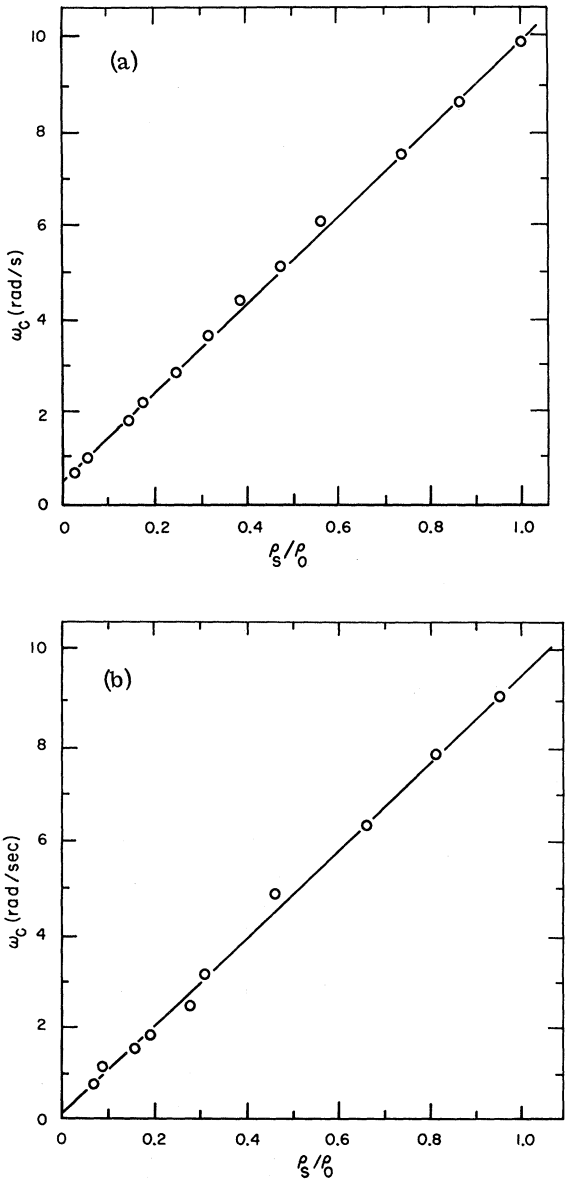

FIG. 14. Critical angular velocity ω_c obtained for flow through 0.20 and 0.05-μ pores [Figs. 14(a) and 14(b), respectively] is plotted against ρ_s/ρ_0, where the superfluid density ρ_s is measured in the same material and ρ_0 is the value of ρ_s at a temperature 25 mdeg below the bulk transition temperature.

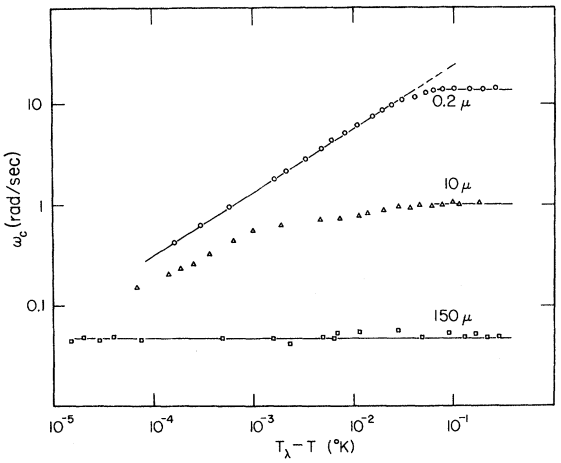

FIG. 15. Effective critical velocity ω_c is shown as a function of $T_\lambda - T$ for flow through 0.2-, 10-, and 150-μ pores. In the case of the 0.2-μ data, T_λ is taken as a temperature 5.0×10^{-4} °K below the bulk transition temperature. With such a λ-point depression, the data for this bucket exhibit an interesting power-law dependence in the critical region near T_λ: $\omega_c = B(T_\lambda - T)^b$ where $B = 1.13\times10^2$ rad/sec and $b = 0.68\pm0.03$.

portional to ρ_s. [See Figs. 14(a) and 14(b).] The critical curves for the larger pore sizes appear to join this curve very near T_λ but our data are insufficient in this extreme region to say so conclusively. (See Figs. 13 and 15.) The data for the 1.20- and 10.0-μ buckets appear to bend away from being perfectly flat before reaching the intrinsic critical velocity curve, but the departure might not be a real one. The channels are not all of uniform size, and the really small ones reach the intrinsic critical velocity curve first as T_λ is approached. Thus, a measure of ρ_s would not be completely reversible as there would be a critical velocity attenuation in the smallest channels only. In some runs, this lack of reversibility was noted—particularly at high speeds near the critical curve and in the smallest channels.[25] Another possible cause of nonreversilbity and even nonreproducibility in some cases is that the currents might be less stable under these conditions and decay. More recent experiments of Kukich, Henkel, and Reppy show that behavior of this type is observed and has a predicted time dependence.[26] Our persistent currents in larger pore sizes were usually stable for periods longer than necessary for our measurements of ρ_s.

In the 0.20-μ bucket very near T_λ, we observed another departure from the $\frac{2}{3}$-power-law behavior. In this case, a very small current seems to persist which we believe to be due to the few larger channels which are always present—such as around the periphery of the container. That is, for these larger channels, the intrinsic critical velocity curve is not reached until an extremely close approach to T_λ is made (closer than our temperature resolution makes possible). The size of such currents is extremely small—less than a millionth as big as the largest currents we observed and this suggests that the number of such channels is very small.[27]

VIII. CONCLUSION

These measurements of persistent currents are completely isothermal. No work is done to push the fluid through the channels. Since the current is in a persistent mode, no heat is dissipated to change the temperature.

The data for ω_c show something new about critical velocities. Near the λ point the critical velocity drops rapidly to zero with a $\frac{2}{3}$-power-law dependence on ΔT, and is independent of the channel size. The effective λ point is depressed relative to that of bulk liquid, and the amount of the depression increases the smaller the channel size. Thus, the critical velocity curves for smaller channels cross over the curves for the larger channels when plotted in terms of the absolute temperature. Therefore, it follows that the critical velocity very near the bulk λ point is smaller for smaller channels. This is the inverse of the situation at lower temperatures where v_c is temperature independent and obeys the approximate relation $v_c d = 10^{-3}$. In this sense, smaller channels resist flow to superfluid more than do the larger ones. This is somewhat like the region above T_λ where the fluid is all normal fluid and is a viscous liquid.

Our measurements of ρ_s are for nonzero velocities. Recent measurements of ρ_s by an independent method support the $\frac{2}{3}$ power behavior for zero velocity.[28] Thus, our measurements show that ρ_s is velocity independent to first order—in keeping with the two-fluid model of He II.

ACKNOWLEDGMENT

One of us (J. R. C.) wishes to thank his thesis advisor Professor C. T. Lane for encouragement and helpful assistance during this research effort.

*Research supported by the National Science Foundation and the U. S. Army Research Office (Durham).

†Thesis of James R. Clow submitted in partial fulfillment of the Doctor of Philosophy degree, Yale University, 1967 (unpublished).

‡Present address: Physics Department, Massachusetts Institute of Technology, Cambridge, Mass. 02139.

§Present address: Laboratory of Atomic and Solid State Physics, Cornell University, Ithaca, N.Y. 14850.

[1]H. E. Hall, Phil. Trans. Roy. Soc. (London) A250, 980 (1957).

[2]W. F. Vinen, Proc. Roy. Soc. (London) A260, 218

(1961).
[3]Philip J. Bendt, Phys. Rev. 127, 1441 (1962).
[4]D. Depatie, J. D. Reppy, and C. T. Lane, in *Proceedings of the Eighth International Congress on Low Temperature Physics, London,* 1962, edited by R. O. Davies (Butterworths, London, 1963).
[5]J. R. Clow and J. D. Reppy, Phys. Rev. Letters 16, 887 (1966).
[6]J. R. Clow and J. D. Reppy, Phys. Rev. Letters 19, 289 (1967).
[7]For a recent summary on this subject, see L. P. Kadanoff, Rev. Mod. Phys., 39, 395 (1967). 39, 395
[8]B. Widom, J. Chem. Phys. 43, 3892, (1965); 43, 3898 (1965).
[9]L. P. Kadanoff, Physics 2, 263 (1966).
[10]C. F. Kellers, Ph. D. thesis (Duke University, 1960) (unpublished); and M. J. Buckingham and W. M. Fairbanks, in *Progress in Low Temperature Physics*, edited by C. J. Gorter (North-Holland, Amsterdam, 1961), Vol. 3, p. 80.
[11]B. D. Josephson, Phys. Letters 21, 608 (1966).
[12]W. E. Keller and E. F. Hammel, Physics 2, 221 (1966).
[13]J. S. Langer and M. E. Fisher, Phys. Rev. Letters 19, 560 (1967).
[14]Similar gyroscope experiments are reported by J. B. Mehl and W. Zimmerman, Jr., Phys. Rev. Letters 14, 815 (1965).
[15]J. R. Clow, D. A. Depatie, J. C. Weaver, and J. D. Reppy, in *Proceedings of the Ninth International Conference on Low Temperature Physics, Columbus, Ohio,* 1964, edited by J. G. Daunt (Plenum, New York, 1964).
[16]This is not strictly true however. Persistent currents can and do decay spontaneously with time. See G. Kukich, R. P. Henkel, and J. D. Reppy, Phys. Rev. Letters 21, 197 (1968).
[17]This method of determining ω_c was first described by J. B. Mehl and W. Zimmerman, Jr., Bull. Am. Phys. Soc. 11, 479 (1966).
[18]The 150-μ bucket contains Scott foam. All others contain Metricel filter material. Metricel filters are manufactured by the Gelman Instrument Company, Ann Arbor, Michigan. The filters are of the triacetate G. A. series and are rated by the manufacturer to have 85% open volume for all sizes.
[19]F. G. Brickwedde *et al.*, Natl. Bur. Std. (U. S.) Monograph No. 10 (U. S. GPO, Washington, D. C, 1960).
[20]For a schematic and description of the operation of the thermometer-control system, see J. R. Clow, Ph. D. thesis (Yale University, 1967) (unpublished).
[21]P. J. Bendt, R. D. Cowan, J. L. Yarnell, Phys. Rev. 113, 1386 (1959).
[22]J. G. Dash and R. D. Taylor, Phys. Rev. 105, 7 (1957).
[23]A. J. Symonds, D. F. Brewer, and A. L. Thomson, in *Quantum Fluids*, edited by D. F. Brewer (Interscience, New York, 1966), p. 267.
[24]A preliminary report of this method was reported by J. D. Reppy and J. R. Clow, in *Proceedings of the Tenth International Conference on Low Temperature Physics, Moscow,* 31 *August*-6 *September*, 1966, edited by M. P. Malkov (Proizvodstrenno-Izdatel' skii Kombinat Moscow, 1967); see also J. D. Reppy, Phys. Rev. Letters 14, 733 (1965).
[25]Note in particular the second curve from the top in Fig. 13. This curve was demonstrated to be nonreversible with about a 10% loss or more, depending on how close an approach was made to the intrinsic critical velocity curve.
[26]G. Kukich, R. P. Henkel, and J. D. Reppy, Phys. Rev. Letters 21, 197 (1968).
[27]ρ_s/ρ in small pores as measured by fourth-sound techniques has also been seen to drop below the bulk value. See, for instance, I. Rudnick, E. Guyon, K. A. Shapiro, and S. A. Scott, Phys. Rev. Letters 19, 488 (1967).
[28]J. A. Tyson and D. H. Douglass, Jr., Phys. Rev. Letters 17, 472 (1966).

PHYSICAL REVIEW A VOLUME 5, NUMBER 1 JANUARY 1972

Ion Drift Velocities in Gaseous Mixtures at Arbitrary Field Strengths*

E. A. Mason and Hong-sup Hahn
Brown University, Providence, Rhode Island 02912
(Received 9 August 1971)

A momentum-transfer theory is used to obtain an expression for the drift velocity of an ion in a multicomponent gas mixture. This is combined with an approximate calculation of the partition of the ion energy in the mixture to yield a formula for the drift velocity in terms of the drift velocities in the pure component gases. Positive deviations from Blanc's law at high fields are predicted, of magnitudes that should be easily measured experimentally.

I. INTRODUCTION

The purpose of this paper is to find an expression for the drift velocity of an ion in a gas mixture, in terms of the drift velocities in the pure component gases. Despite its obvious practicality, the problem has apparently been little studied, except at very low electric fields where the drift velocity is directly proportional to the field strength. In this regime Blanc's law[1,2] holds,

$$1/K_{\text{mix}} = \sum_j x_j/K_j \,, \tag{1}$$

where the x_j are mole fractions and the K_j are the mobilities in the pure component gases at the same total number density as the mixture. If the ion retains its identity in the mixture, deviations from Blanc's law are usually small.[3] The behavior at higher field strengths does not seem to be known.